

Analysis and kinematic optimization of planar 2-DOF 5R parallel mechanisms considering the force transmissibility

Xin-Jun Liu ^a, Jinsong Wang ^a, Markus Wabner ^b and Reimund Neugebauer ^b

^a Institute of Manufacturing Engineering, Department of Precision Instruments, Tsinghua University, Beijing, 100084, P.R. of China. Email: xinjunliu@mail.tsinghua.edu.cn

^b Fraunhofer Institute for Machine Tools and Forming Technology IWU, Reichenhainer Str. 88, D-09126, Chemnitz, Germany

Abstract

This paper treats the problems of kinematic analysis and optimization of the 5R symmetrical parallel mechanism taking into account the force transmissibility. In the design process, the theoretical workspace cannot be used practically due to the inside singularity. The usable workspace without singularity inside cannot still be useful in an optimization problem since a mechanism at and near the boundary of the workspace will be out of control. The local conditioning index (LCI), which is widely used in the field of serial robots and has been applied in many optimizations, has the problem of physical significance and difficulty of measuring the distance to a singularity of a parallel mechanism. For such reasons, the concept of transmission angle is introduced in this paper to the optimization of the planar 5R parallel mechanisms. Based on this concept, three new indices are proposed. After presenting the performance charts, the optimization process of the mechanisms is finally presented by considering the workspace and force transmissibility.

Keywords: Parallel mechanism; Optimization; Performance chart; Workspace; Singularity

1. Introduction

Analysis and kinematic design are two important issues in the development of a parallel mechanism. Without exhaustive analysis, a design will not be perfect or even will be lost. Then, analysis is primary. In the design process, kinematics and workspace are two typical problems since they are the basic model and reference to define and evaluate the performances of a mechanism. For such a reason, the kinematics and workspace are the most studied issues in the field [1-6]. The efforts were motivated by the fact that they would be finally applied to the design and application of the devices.

Kinematic optimization is one of the most important and challenging problems in the design of parallel kinematics, and is increasingly attracting the attention of researchers [7]-[9]. There are two issues involved: performance evaluation and dimension synthesis. Having designed a mechanism, it is necessary to evaluate its performances. A second problem is to determine the dimensions (link lengths) of the mechanism, which is suitable for the task at hand. The latter one is one of the most difficult issues in this field.

Several well-defined performance indices, such as workspace [8], singularity [7], dexterity [10,11], accuracy [12], stiffness [13], and conditioning index [7], have been extensively developed and applied to both serial and parallel mechanisms. A recent study [14] reviewed the most common of these indices that have been applied in the optimum design of parallel mechanisms: the condition number [10] of the Jacobian matrix and the global conditioning index (GCI) [15]. The study found serious inconsistencies when these

indices are applied to parallel mechanisms with combined translational and rotational degrees of freedom, and concluded that these indices should not be used in parallel mechanisms with mixed types of degrees of freedom (translational and rotational). What is more, to eliminate the singularity and its near configurations, most researchers used the local conditioning index (LCI) [15]. Usually, a good-condition workspace or effective workspace was defined with respect to a specified minimum LCI [9,16]. However, the minimum is still arbitrary or comparative since we cannot give it a definite value. Generally, it is not possible to define a mathematical distance to a singularity for a parallel mechanism [14]. Instead of LCI, another index will be defined in this paper.

As is well known, the *transmission angle* is an important index for the design of a planar four-bar mechanism as was pointed out by Alt [17], who defined the concept, using the forces tending to move the driven link and tending to apply pressure to the driven link bearings as a simple index, to judge the force-transmission characteristics of a mechanism. By means of the index of *transmission angle*, the quality of motion/force transmission in a mechanism can be judged in the design stage. Therefore, the *transmission angle* is an index evaluating the quality of motion/force transmission. It helps to decide the "best" from among a family of possible mechanisms for the most effective force transmission [18]. Actually, a good *transmission angle* is the solution to most of the problems in planar mechanisms. For example, Alt [17] used the transmission angle to isolate better chains for various linkage applications. As is pointed out in [19], though a good *transmission angle* is not a cure-all for every design problem, for many mechanical applications it can guarantee the performance of a linkage at higher speed without unfavorable vibrations.

The study in [20] shows that when the *transmission angle* is equal to 90° , the most effective force transmission takes place and the output motion becomes less sensitive to the manufacturing tolerances on the link lengths, clearance between joints, and change of dimensions due to thermal expansion. Mechanisms having a *transmission angle* too far from 90° exhibit poor operational characteristics such as noise and jerk at high speeds [21,22]; and if it is 0, self-locking takes place. Thus the *transmission angle* of a mechanism provides a very good indication of the quality of its motion, the accuracy of its performance, its expected noise output, and its costs in general [23]. A large *transmission angle* usually leads to reasonable mechanical advantages and a high quality of motion transmission. The study of link mechanisms shows that *transmission angle* is significant not only as an indicator of good force and motion transmission but also as a prime factor in the linkage sensitivity to small design parameter errors. The smaller the *transmission angle*, the more sensitive the linkage will be [24]. In [18], the authors gave a summary description of the effect of transmission angle on velocity, input crank angle, friction, mechanical advantage, velocity, tolerance, clearance, and performance sensitivity. Many studies have reached the conclusion that if the *transmission angle* becomes too small, the mechanical advantage becomes small, and even a very small amount of friction will cause the mechanism to jam. For the purpose of high speed, high accuracy, and high quality of motion transmission, the most widely accepted design limits for the transmission angle are $(45^\circ, 135^\circ)$ [21] or $(40^\circ, 140^\circ)$ [17].

A planar four-bar mechanism is a single-closed-loop system. A parallel mechanism belongs to the multi-closed-loop mechanism group. Usually, a fully parallel mechanism has more or less the characteristic of a planar four-bar mechanism. We suggest that the design concept of the four-bar mechanisms could be used in the design of a parallel mechanism.

Many methods have been proposed for the dimension optimization of specified

mechanisms. The most common one is the objective-function-based optimal design [8,13,16]. According to this methodology, an objective function with specified constraints must be established, and then a search conducted to find the result utilizing an optimization algorithm. Not only is this method time-consuming, but it is difficult to reach the globally optimum target because of the non-finiteness of the individual parameters, the antagonism of multiple criteria and the assignment of its initial value. The most serious drawback is that it provides only one solution for a design problem. This is actually a fatal one for practical design purposes, since it is impossible to predict any application condition in advance and very difficult to be sure that a particular design is the only possible solution for a given problem. The ideal dimension optimization method, or optimal method, would be the performance chart (atlas), which is widely used in classical design and in most design manuals. A performance atlas can show, globally and visually, the relationship between a performance index and the associated design parameters in a limited space [25]. Moreover, it can show how antagonistic the involved indices actually are. Compared with the result achieved by the objective-function-based method, the optimal method result is comparative and fuzzy. However, it is more flexible, due to the fact that it provides not only a single solution, but all possible solutions to a design problem. This means that the designer can adjust the optimum result appropriately according to the particular design conditions he is dealing with [25].

The five-bar mechanism is a typical parallel mechanism with the minimal degrees of freedom (DoFs) in the field, which can be used for positioning a point on a region of a plane that is known as the workspace. The 5R (R-revolute joint) parallel mechanism consists of five bars that are connected end to end by five revolute joints, two of which that are connected to the base are actuated. Such a mechanism with a symmetric structure attracted many researchers, who have investigated its position analysis [26], workspace [27, 28], assembly modes [28], singularity [27, 29], performance atlases [28, 30] and kinematic design [30]-[32]. What is more, the symmetrical mechanism has been applied in the development of the MELFA RP Series robots in the Mitsubishi Electric Corporation. In this paper, based on the concept of *transmission angle*, three indices will be introduced to analyze and design the planar 2-DOF 5R parallel mechanisms. In order to study all possible 5R parallel mechanisms, a design space is established according to the concept in [24]. The design space is used to investigate the indices of each parallel mechanism systematically.

The remainder of this paper is organized as follows. The next section describes the kinematic problems of the planar 2-DOF 5R parallel mechanism. Section 3 introduces the parameter design space of the mechanisms. Section 4 recalls the traditional analysis, including theoretical workspace, Jacobian matrix, singularity and usable workspace. The concept of transmission angle is presented in section 5. Section 6 gives the definition of some indices, i.e. local transmission index (LTI), good-transmission workspace (GTW), and global transmission index (GTI). In section 7, the performance charts of the mechanisms have been represented. Section 8 presents the optimization process of the mechanisms using the obtained performance charts. Conclusions are given in the last section.

2. Kinematic problems

The planar 5R parallel mechanism, as shown in Fig. 1(a), is such a mechanism that the output point is connected to the base by two legs, each of which consists of three revolute joints and two links. The two legs are connected to a common point with the common

revolute joint at the end of each leg. In each of the two legs, the revolute joint connected to the base is actuated. Such a mechanism can position a point freely in a plane.

A kinematics model of the mechanism is developed as shown in Fig. 1(b). Each actuated joint is denoted as A_i ($i=1, 2$), the other end of each actuated link is denoted as B_i and the common joint of the two legs is denoted as P , which is also the output point. A fixed global reference system $O-xy$ is located at the center of A_1A_2 with the y -axis normal to A_1A_2 and the x -axis directed along A_1A_2 . For the structure symmetry, there are $OA_1=OA_2$, $OA_1=OA_2$ and $B_1P=B_2P$. The length of the actuated link for each leg is denoted as $A_iB_i=R_1(r_1)$. Additionally, $B_iP=R_2(r_2)$ and $OA_i=R_3(r_3)$. Here, R_j ($j=1,2,3$) are link lengths with dimension and r_j ($j=1,2,3$) are those with non-dimension.

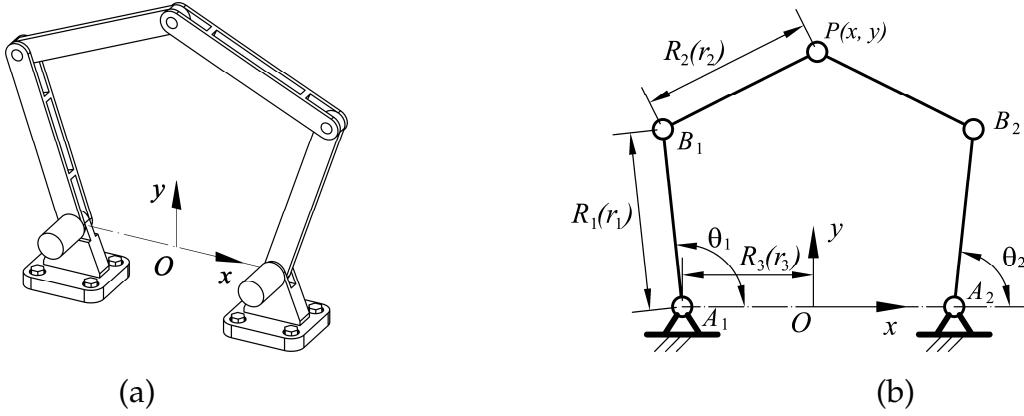


Fig. 1 The planar 5R parallel mechanism

2.1 Inverse kinematics

The position of the output point P in the reference system $O-xy$ can be described by the position vector \mathbf{p} , and there is

$$\mathbf{p} = (x \quad y)^T \quad (1)$$

In the reference frame $O-xy$, the position vectors \mathbf{b}_i of points B_i ($i=1, 2$) can be written as

$$\mathbf{b}_1 = (r_1 \cos \theta_1 - r_3 \quad r_1 \sin \theta_1)^T \quad \text{and} \quad \mathbf{b}_2 = (r_1 \cos \theta_2 + r_3 \quad r_1 \sin \theta_2)^T \quad (2)$$

where θ_1 and θ_2 are the input angles of the two legs. Then, the inverse kinematic problem can be solved by writing following constraint equation

$$|\mathbf{p}\mathbf{b}_i| = r_2, \quad i = 1, 2 \quad (3)$$

in another form

$$(x - r_1 \cos \theta_1 + r_3)^2 + (y - r_1 \sin \theta_1)^2 = r_2^2 \quad (4)$$

$$(x - r_1 \cos \theta_2 - r_3)^2 + (y - r_1 \sin \theta_2)^2 = r_2^2 \quad (5)$$

from which, if the position of output point P is known, the inputs to reach the position can be obtained as

$$\theta_i = 2 \tan^{-1}(z_i), \quad i = 1, 2 \quad (6)$$

where

$$z_i = \frac{-b_i + \sigma_i \sqrt{b_i^2 - 4a_i c_i}}{2a_i}, \quad i = 1, 2 \quad (7)$$

in which

$$\sigma_i = 1 \text{ or } -1$$

$$a_1 = r_1^2 + y^2 + (x + r_3)^2 - r_2^2 + 2(x + r_3)r_1$$

$$b_1 = -4yr_1$$

$$c_1 = r_1^2 + y^2 + (x + r_3)^2 - r_2^2 - 2(x + r_3)r_1$$

$$a_2 = r_1^2 + y^2 + (x - r_3)^2 - r_2^2 + 2(x - r_3)r_1$$

$$b_2 = b_1 = -4yr_1$$

$$c_2 = r_1^2 + y^2 + (x - r_3)^2 - r_2^2 - 2(x - r_3)r_1$$

From Eq.(7), one can see that there are four solutions for the inverse kinematic problem of the 5R mechanism. The configuration shown in Fig.1 can be obtained if $\sigma_1 = 1$ and $\sigma_2 = -1$. Such a configuration is denoted as the “+ -” model. Then there are three others, which are “- +”, “- -”, and “++” models, respectively. These four inverse kinematics models correspond to four types of working modes.

2.2 Forward kinematics

The Forward kinematic problem is to obtain the output with respect to a set of given inputs. From Eqs.(4) and (5), one obtains

$$x^2 + y^2 - 2(r_1 \cos \theta_1 - r_3)x - 2r_1 \sin \theta_1 y - 2r_1 r_3 \cos \theta_1 + r_3^2 + r_1^2 - r_2^2 = 0 \quad (8)$$

$$x^2 + y^2 - 2(r_1 \cos \theta_2 + r_3)x - 2r_1 \sin \theta_2 y + 2r_1 r_3 \cos \theta_2 + r_3^2 + r_1^2 - r_2^2 = 0 \quad (9)$$

Eq.(8)-Eq.(9) yields

$$x = ey + f \quad (10)$$

in which $e = \frac{r_1(\sin \theta_1 - \sin \theta_2)}{2r_3 + r_1 \cos \theta_2 - r_1 \cos \theta_1}$ and $f = \frac{r_1 r_3(\cos \theta_2 + \cos \theta_1)}{2r_3 + r_1 \cos \theta_2 - r_1 \cos \theta_1}$. Substituting Eq.(10) to

Eq.(8) yields

$$dy^2 + gy + h = 0 \quad (11)$$

where

$$d = 1 + e^2$$

$$g = 2(ef - er_1 \cos \theta_1 + er_3 - r_1 \sin \theta_1)$$

$$h = f^2 - 2f(r_1 \cos \theta_1 - r_3) - 2r_1 r_3 \cos \theta_1 + r_3^2 + r_1^2 - r_2^2$$

Then, y can be obtained from Eq.(11) as

$$y = \frac{-g + \sigma \sqrt{g^2 - 4dh}}{2d} \quad (12)$$

in which $\sigma = 1$ or -1 . From Eqs. (10) and (12), one sees that there are two solutions for the forward kinematic problem of the mechanism. They correspond to types of assembly modes. The corresponding configurations are called the *up-* and *down-configurations*. The *up-configuration* can be achieved when $\sigma = 1$.

For example, if $r_1 = 1.2$, $r_2 = 1.0$ and $r_3 = 0.8$, the four inverse kinematic models of the mechanism are shown in Fig.2, where the specified position of the output point is $(x = -0.37, y = 1.44)$. And the two forward kinematic models are shown in Fig.3, where the inputs are given as $\theta_1 = 4\pi/9$ and $\theta_2 = 7\pi/18$.

In this paper, what we are concerned about is the mechanism with the “+ -” model and, at the same time, the *up-configuration*.

3. Design space of the 5R parallel mechanisms

As it is well known, the performance of a parallel mechanism depends on not only the

pose of the moving platform but also the link lengths (dimensions). Disregarding the pose, each of the links can be the length between zero and infinite. And there are always several links in a parallel mechanism. Then the combination of the links with different lengths will be infinite. They undoubtedly have different performance characteristics. To apply a specified mechanism in practice, we usually should determine the link lengths with respect to a desired application. This is actually the so-called optimum design (parameter synthesis) of the mechanism. In such a process, one of the most classical tools that has been using is the chart, which can show the relationship between performances and link lengths. To make it work, we should first develop a space that contains all involved links. Next is to plot the chart considering a desired performance. In this paper, the space is referred to as *the design space*. The chart that can show the relationship between performances and link lengths is referred to as *atlas*. The *index* is used to evaluate a performance. Normally, several indices will be considered in the design process.

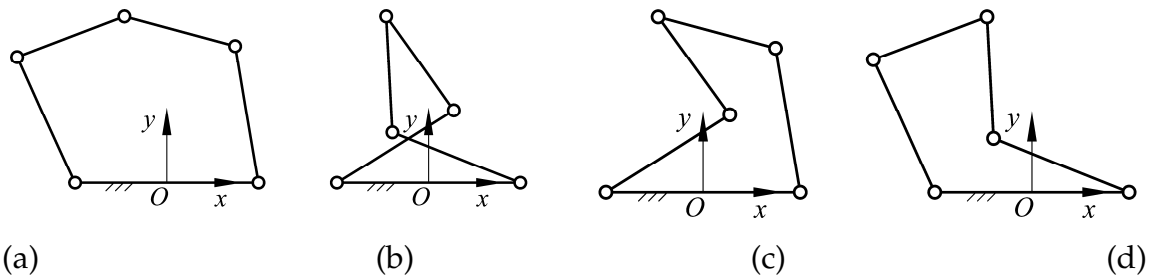


Fig. 2 The four inverse kinematic models: (a) “+ -” model; (b) “- +” model; (c) “- -” model; (d) “+ +” model

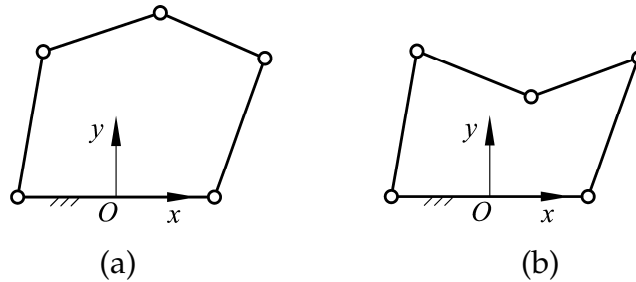


Fig. 3 The two forward kinematic models: (a) the up-configuration; (b) the down-configuration

For the parallel mechanism considered here, due to the symmetric structure, there leaves three parameters, which are R_1 , R_2 and R_3 as shown in Fig.1. Any one of the parameters R_1 , R_2 and R_3 can have any value between zero and infinite. This is the biggest difficulty to develop a design space that can embody all mechanisms (with different link lengths) within a finite space. For this reason, we must eliminate the physical link size of the mechanisms [25]. Let

$$D = (R_1 + R_2 + R_3)/3 \quad (13)$$

One can obtain 3 non-dimensional parameters r_i by means of

$$r_1 = R_1/D, \quad r_2 = R_2/D, \quad r_3 = R_3/D \quad (14)$$

This would then yield

$$r_1 + r_2 + r_3 = 3 \quad (15)$$

Theoretically, from Eq.(15), the three non-dimensional parameters r_1 , r_2 and r_3 can have any value between 0 and 3. For the 5R parallel mechanism studied here, the analysis

on the workspace and singularity shows that r_1 and r_2 cannot be 0 and r_1+r_2 cannot be less than r_3 , otherwise they will result in the failure of mechanism assembly. Therefore, the three parameters should be

$$0 < r_1, r_2 < 3 \text{ and } 0 \leq r_3 \leq 1.5 \quad (16)$$

Based on Eqs. (15) and (16), one can establish a design space as shown in Fig. 4(a), in which the trapezoid $ABCD$ is actually the design space. In Fig. 4(a), the trapezoid $ABCD$ is restricted by r_1 , r_2 and r_3 . Therefore it can be figured in another form as shown in Fig. 4(b), which is referred to as the planar-closed configuration of the design space.

For convenience, two orthogonal coordinates s and t are utilized to express r_1 , r_2 and r_3 . Thus, by using

$$\begin{cases} s = 2r_1/\sqrt{3} + r_3/\sqrt{3} \\ t = r_3 \end{cases} \quad (17)$$

coordinates r_1 , r_2 and r_3 can be transformed into s and t . Eq. (17) is useful for constructing a performance atlas.

In order to study the performance of the parallel mechanism in detail, five lines $r_1=r_3$, $r_2=r_3$, $r_2=r_1+r_3$, $r_1=r_3+r_2$ and $r_1=r_2$ can be used to divide the design space into 10 sub-regions, i.e., Ia, Ib, IIa, IIb, IIIa, IIIb, IVa, IVb, Va and Vb, as shown in Fig. 4(b). The former four lines indicate four types of change point mechanisms, respectively. The reason why $r_1=r_2$ is also used is that if $r_1=r_2$ the boundaries of the theoretical workspace are only two circles C_{10} and C_{20} . Such a design space will help us to investigate detailed the performance characteristics of all 5R parallel mechanisms with possible combinations of $R_1(r_1)$, $R_2(r_2)$ and $R_3(r_3)$.

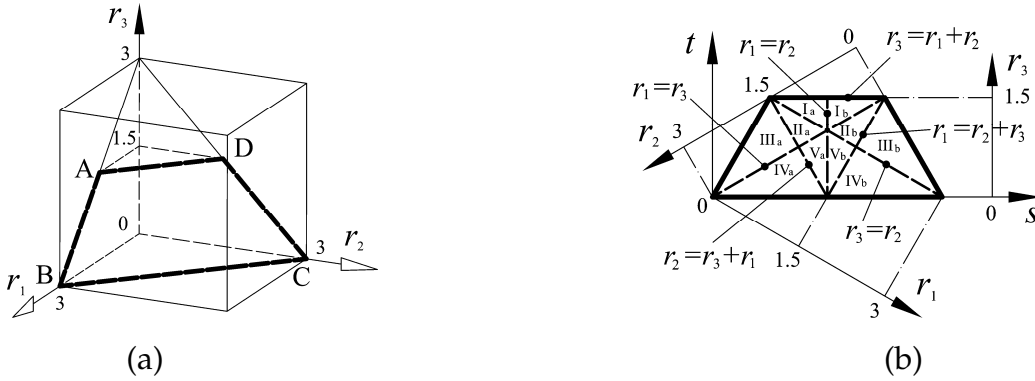


Fig. 4 The design space of the 5R parallel mechanism

4. Traditional analysis

Some problems, such as workspace, Jacobian matrix and singularity, have been analyzed in Ref. [27]. Here, for convenience, we recall these problems.

4.1 Theoretical workspace

Theoretical workspace is defined as the region that the output point can reach if θ_i changes from 0 to 2π without the consideration of interference between links and the singularity.

From Eq. (4), one can see that if θ_1 is specified, the workspace of the first leg is a circle centered at the point $(r_1 \cos \theta_1 - r_3, r_1 \sin \theta_1)$ with a radius of r_2 . The circle is denoted as C_{11} . If θ_i changes from 0 to 2π , the center point is located at a circle

centered at point $A_1(-r_3, 0)$ with a radius of r_1 . The circle is denoted as C_{12} . Then, the workspace of the leg is the enveloping region of the circle C_{11} when its center rolls at the circle C_{12} . Actually, the enveloping region is an annulus bounded by two following circles

$$C_{1o}: (x+r_3)^2 + y^2 = (r_1+r_2)^2 \quad (18)$$

$$C_{1i}: (x+r_3)^2 + y^2 = (r_1-r_2)^2 \quad (19)$$

For the second leg, the workspace is an annulus bounded by circles

$$C_{2o}: (x-r_3)^2 + y^2 = (r_1+r_2)^2 \quad (20)$$

$$C_{2i}: (x-r_3)^2 + y^2 = (r_1-r_2)^2 \quad (21)$$

When $r_1 = r_2$ the workspaces are two circles defined by Eqs. (18) and (20), respectively. The theoretical workspace of the mechanism is the intersection of the two annuluses. For example, the workspace of a mechanism with $r_1 = 1.2$, $r_2 = 1.0$ and $r_3 = 0.8$ is shown as the hatched region in Fig. 5, where the boundaries are also illustrated.

From above analysis, one can see that if $r_3 > r_1 + r_2$, there is no intersection, i.e., no workspace. Especially, if $r_3 = r_1 + r_2$, the workspace is only one point, which is the center of the line segment A_1A_2 .

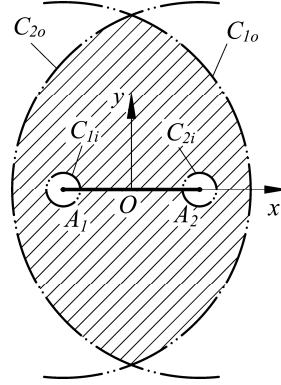


Fig. 5 Theoretical workspace is shown as the hatched region

4.1.1 Performance chart of the theoretical workspace area

The theoretical workspace can be determined based on Eqs. (18)-(21). The chart for the theoretical workspace area is shown in Fig. 6, from which one can see that

- The theoretical workspace area is inverse proportional to parameter r_3 ;
- The area atlas is symmetric with respect to $r_1 = r_2$, which means that the area of a mechanism with $r_1 = a$, $r_2 = b$ ($a, b < 3$) and $r_3 = 3 - a - b$ is identical to that of a mechanism with $r_1 = b$, $r_2 = a$ ($a, b < 3$) and $r_3 = 3 - a - b$;
- When $r_3 = 1.5$ (or $r_1 + r_2 = r_3$), the area is 0;
- The area reaches its maximum value when $r_1 = r_2 = 1.5$ and $r_3 = 0$. The maximum value is 9π .

4.1.2 Distribution characteristics of the theoretical workspace shape in the design space

Meanwhile, we can also obtain the workspace of a typical mechanism in each of the 10 sub-regions. The distribution characteristics of the workspace shape can be summarized based on these workspaces. The distribution in the design space is shown in Fig. 7, from which one can see that the distribution is symmetric with respect to the line $r_1 = r_2$. This means that the theoretical workspace shape of a mechanism with $r_1 = a$, $r_2 = b$ ($a, b < 3$)

and $r_3 = 3 - a - b$ is the same as that of a mechanism with $r_1 = b$, $r_2 = a$ ($a, b < 3$) and $r_3 = 3 - a - b$. This characteristic is what it should be, as the radii of boundary circles C_{1o} , C_{2o} , C_{1i} and C_{2i} of the theoretical workspace are just related to $r_1 + r_2$ and $|r_1 - r_2|$. Then there are only five types of theoretical workspace shapes for the 5R parallel mechanism. What is more, each theoretical workspace is symmetric about the x and y axes.

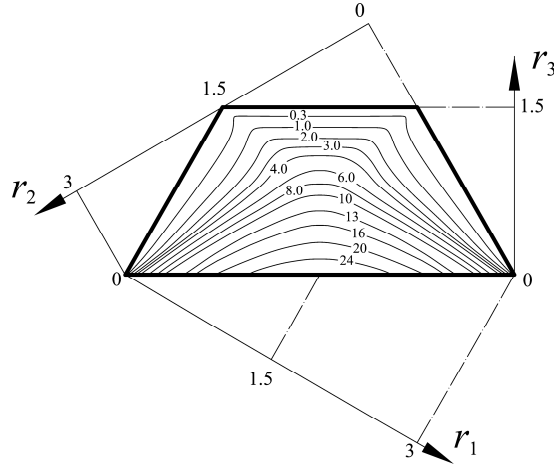


Fig. 6 Performance chart of the theoretical workspace area

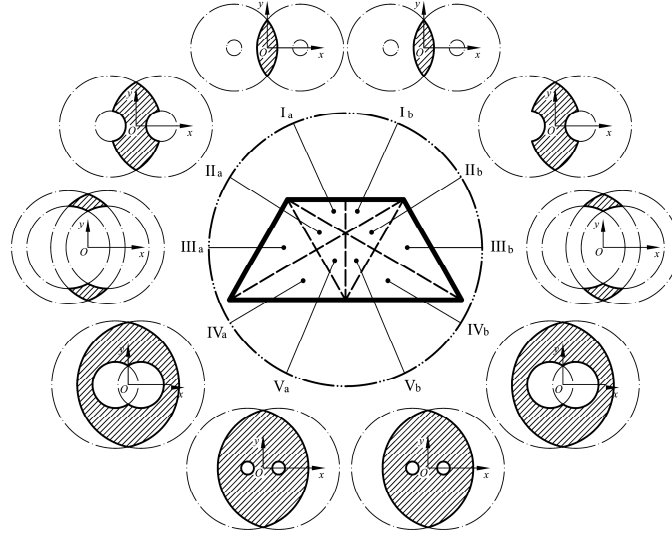


Fig. 7 Distribution of the theoretical workspace shape in the design space

4.2 Jacobian Matrix

Equations (4) and (5) can be differentiated with respect to time to obtain the velocity equations, which yields

$$r_1 [y \cos \theta_1 - (x + r_3) \sin \theta_1] \dot{\theta}_1 = (x + r_3 - r_1 \cos \theta_1) \dot{x} + (y - r_1 \sin \theta_1) \dot{y} \quad (22)$$

$$r_1 [y \cos \theta_2 + (r_3 - x) \sin \theta_2] \dot{\theta}_2 = (x - r_3 - r_1 \cos \theta_2) \dot{x} + (y - r_1 \sin \theta_2) \dot{y} \quad (23)$$

Rearranging Eqs.(22) and (23) leads to an equation of the form

$$A \dot{\theta} = B \dot{p} \quad (24)$$

where \dot{p} is the vector of output velocities defined as

$$\dot{\mathbf{p}} = (\dot{y} \quad \dot{z})^T \quad (25)$$

and $\dot{\boldsymbol{\theta}}$ is the vector of input velocities defined as

$$\dot{\boldsymbol{\theta}} = (\dot{\theta}_1 \quad \dot{\theta}_2)^T \quad (26)$$

Matrices A and B are, respectively, the 2×2 matrices of the mechanism and can be expressed as

$$A = \begin{bmatrix} y \cos \theta_1 - (x + r_3) \sin \theta_1 & 0 \\ 0 & y \cos \theta_2 + (r_3 - x) \sin \theta_2 \end{bmatrix} r_1 \quad (27)$$

$$B = \begin{bmatrix} x + r_3 - r_1 \cos \theta_1 & y - r_1 \sin \theta_1 \\ x - r_3 - r_1 \cos \theta_2 & y - r_1 \sin \theta_2 \end{bmatrix} \quad (28)$$

The Jacobian matrix of the mechanism can be written as

$$J = A^{-1}B \quad (29)$$

4.3 Singularity Analysis

4.3.1 Three kinds of singularities

In the parallel mechanism, singularities occur whenever A , B or both, become singular. As a singularity leads to an instantaneous change of the mechanism's DoF, the analysis of parallel mechanisms has drawn considerable attention.

The singularity of the 5R symmetrical parallel mechanism has been studied by many researchers. Here, we summarize this issue as following.

1) The stationary singularity occurs when A becomes singular but B remains invertible. Physically, this corresponds to the configuration whenever one of the legs A_1B_1P and A_2B_2P is completely extended or folded. From the analysis of the workspace, this singularity occurs when the output point P reaches its limit or is at the boundary of the workspace. This singularity is also referred to as the *serial singularity*. For example, for the mechanism with the parameters $r_1 = 1.2$, $r_2 = 1.0$ and $r_3 = 0.8$, some configurations of this kind of singularity are shown in Fig. 8. The loci of this kind of singularity are actually given by circles C_{1o} , C_{1i} , C_{2o} and C_{2i} , as shown in Fig.5. Note that, $r_1 = 0$ leads to $\det(A) = 0$ as well. But this also results the mechanism in an unmovable status.

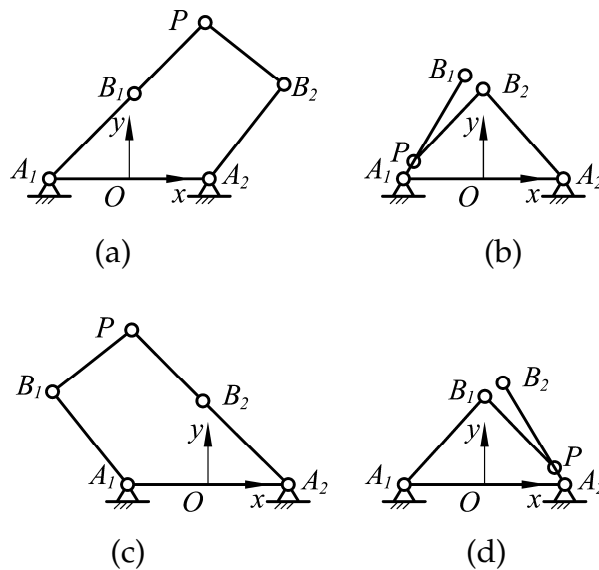


Fig. 8 Some configurations of the stationary singularity:

- (a) the first leg is completely extended; (b) the first leg is completely folded; (c) the second leg is completely extended; (d) the second leg is completely folded.

2) The uncertainty singularity, occurring only in closed kinematics chains, arises when B becomes singular but A remains invertible. Usually, there are two cases for this singularity. The first case is that B_1PB_2 is completely folded, i.e., the points B_1 and B_2 are coincident. Such a configuration is shown in Fig. 9(a), from which one can see that when this condition occurs the locus of the point P is a circle centered at point $(0, \sqrt{r_1^2 - r_3^2})$ or $(0, -\sqrt{r_1^2 - r_3^2})$ with a radius of r_2 , namely,

$$x^2 + \left(y - \sqrt{r_1^2 - r_3^2}\right)^2 = r_2^2 \quad \text{or} \quad x^2 + \left(y + \sqrt{r_1^2 - r_3^2}\right)^2 = r_2^2 \quad (30)$$

Please note that, if $r_3 = 0$, this type of singularity can occur easily when links A_1B_1 and A_2B_2 are coincident as shown in Fig. 9(b). For this case, the loci of point P is an annulus, which is bounded by two circles

$$x^2 + y^2 = (r_1 + r_2)^2 \quad \text{and} \quad x^2 + y^2 = (r_1 - r_2)^2 \quad (31)$$

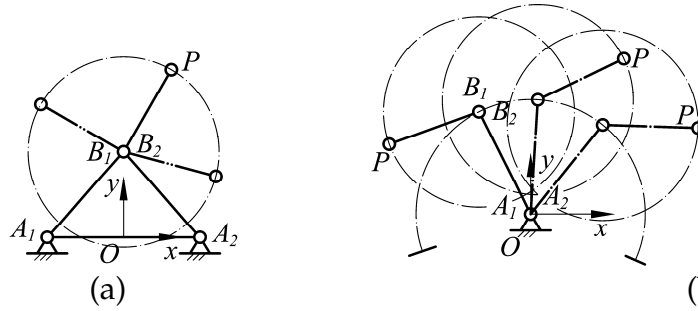


Fig. 9 The configurations when B_1 and B_2 are coincident

The second case is that when B_1PB_2 is completely extended. Such a singular configuration is shown in Fig. 10. The locus of point P for this type of singularity can be described by

$$\begin{cases} x = r_1(\cos \theta_2 + \cos \theta_1)/2 \\ y = r_1(\sin \theta_2 + \sin \theta_1)/2 \end{cases} \quad (32)$$

where

$$\theta_1 \in [0, 2\pi]$$

$$\theta_2 = 2 \tan^{-1}(z)$$

$$z = \left(-b \pm \sqrt{b^2 - 4ac}\right)/(2a)$$

$$a = 4r_2^2 + 4r_1r_3 \cos \theta_1 + 4r_1r_3 - 4r_3^2 - 2r_1^2 - 2r_1^2 \cos \theta_1$$

$$b = 4r_1^2 \sin \theta_1$$

$$c = 4r_2^2 + 4r_1r_3 \cos \theta_1 - 4r_1r_3 - 4r_3^2 - 2r_1^2 + 2r_1^2 \cos \theta_1$$

Based on the analysis in [33], Eq. (32) can be also rewritten as the following sextic:

$$(x + 2r_3)^2(x^2 + 4r_3x + 3r_3^2 + r_2^2 - r_1^2 + y^2)^2 + y^2(x^2 + 4r_3x + 5r_3^2 + r_2^2 - r_1^2 + y^2)^2 - 4r_3^2r_2^2y^2 = 0 \quad (33)$$

For the uncertainty singularity, if $r_1 < r_3$, the singularity that B_1 and B_2 are coincident will not occur. If $r_2 > r_1 + r_3$, there is no the singularity that B_1PB_2 is completely extended.

3) The third kind of singularity occurs when both A and B become simultaneously singular. This singularity is of a slightly different nature than the first two since it is not only configuration but also architecture dependent.

From the analysis on the stationary and uncertainty singularities, one can see that the third kind of singularity occurs when the five points A_1 , B_1 , P , B_2 and A_2 are collinear. There are six cases for this kind of singularity, as shown in Fig. 11. The parameter conditions to those singularities are as following

- (a) $r_1 = r_3$, one singularity is shown in Fig. 11(a);
- (b) $r_2 = r_3$, a corresponding singular configuration is shown in Fig. 11(b);
- (c) $r_3 = r_1 + r_2$, see Fig. 11(c) for the singular configuration;
- (d) $r_2 = r_1 + r_3$, Fig. 11(d) shows such a singularity;
- (e) $r_1 = r_3 + r_2$, see Fig. 11(e);
- (f) $r_3 = 0$, one singular configuration is shown in Fig. 11(f).

The mechanism satisfies any one of the five parameter conditions (a)~(e) is referred to as a *change point mechanism*.

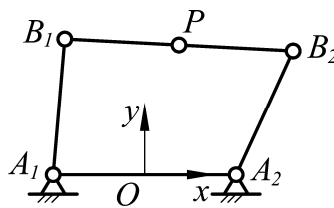


Fig. 10 The configuration when B_1PB_2 is completely extended

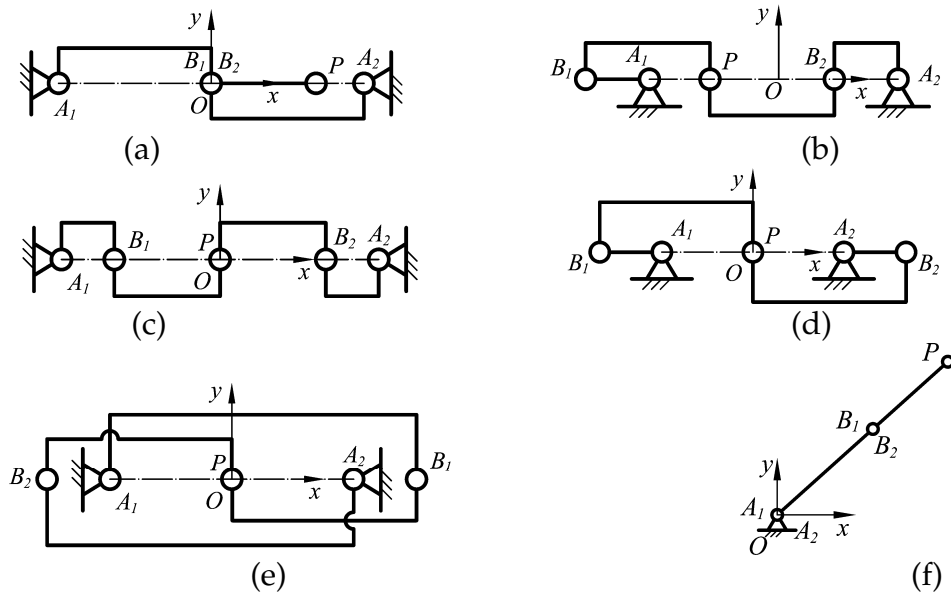


Fig. 11 Five configurations of the stationary singularity

The analysis on the kinematics of the mechanism shows that there are four solutions for the inverse kinematics and two solutions for the forward kinematics. Any one of the singularities will result in the change of solution number of the kinematics. For example, the stationary singularity leads to the loss of solution number of the inverse kinematics. While in the uncertainty singular configuration, the solution number of the forward kinematics can be less or more than two. In the third kind of singularity, both the inverse and forward kinematics will be different. Then the stationary singularity can be called the inverse kinematic singularity, the uncertainty singularity the forward kinematic singularity, and the third kind of singularity the inverse and forward kinematic singularity. Notably, the loci of the uncertainty singularity must be within the workspace.

4.3.2 Distribution of the singular loci in the design space

Based on the analysis on the singularity, there exist two kinds of singular loci. The first kind of locus is the inverse singular locus. The loci are C_{1o} , C_{1i} , C_{2o} and C_{2i} given by Eqs. (18)-(21). They are actually the boundaries of the theoretical workspace. The second one is the forward singular locus. There are two cases for this kind of singular locus. One is that when the points B_1 and B_2 are coincident. The loci are actually two circles given by Eq. (30), which are denoted as C_{Coin-U} and C_{Coin-D} . The second case occurs when B_1PB_2 is completely extended. The locus is presented by Eq. (32) or Eq. (33), which is denoted as C_{Col} . For example, the singular loci of the mechanism with $r_1 = 1.2$, $r_2 = 1.0$ and $r_3 = 0.8$ are shown in Fig. 12.

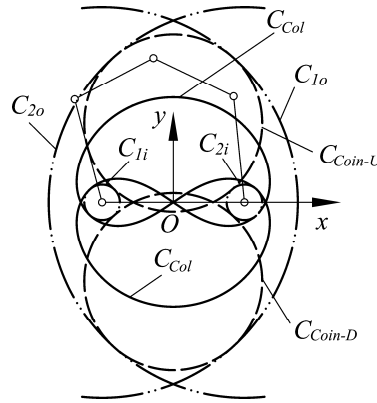


Fig. 12 The singular loci of a mechanism

However, with specified working and assembly modes, a mechanism cannot have all the singularities. According to the singularity analysis, the stationary singularity is actually the boundary of a theoretical workspace. Then, a mechanism with every working mode can have such singular loci. However, as the uncertainty singularity occurs inside the workspace, not every working mode has all such singularities. Normally, for most 5R parallel mechanisms, there are four tangent points between the first and second kinds of singular loci. At these points, the mechanism is in the change point's mechanism. The points can be used to identify which singular loci a specified working mode can have. For example, Fig. 13 shows some singular configurations and singular loci of the mechanism with $r_1 = 1.2$, $r_2 = 1.0$ and $r_3 = 0.8$. As shown in Fig. 13 (a), there are four tangent points m , n , q and k between the singular curve C_{Coin-U} and the first kind of singular loci. At these four points, both of the stationary and uncertainty singularities occur. The four points divide the singular curve C_{Coin-U} into four parts. At the arc $m1n$, the mechanism is in singular only when it is with the "--" mode. At the arcs $n2q$, $q3k$ and $k4m$, the working modes "-+", "++" and "+-" are in singular, respectively. Similarly, at C_{Coin-D} , arcs $m'1'n'$, $n'2'q'$, $q'3'k'$ and $k'4'm'$ are the singular curves for the working modes "++", "+-", "--" and "-+", respectively. For the singular locus C_{Col} , as shown in Fig. 13 (b) and (c), curves $t'5v$, $t'6v$, $t'5'v'$ and $t'7'6'v'$ are the singular loci for the working modes "+-", "++", "-+" and "--", respectively. For the mechanisms in sub-region IVb where $r_1 > r_2 + r_3$ and $r_2 > r_3$, the parameter condition does not allow the case that the singular locus C_{Col} and the first kind of singular locus are tangent to occur. These mechanisms

with the working modes “++” and “--” don't have the singularity that B_1PB_2 is completely extended.

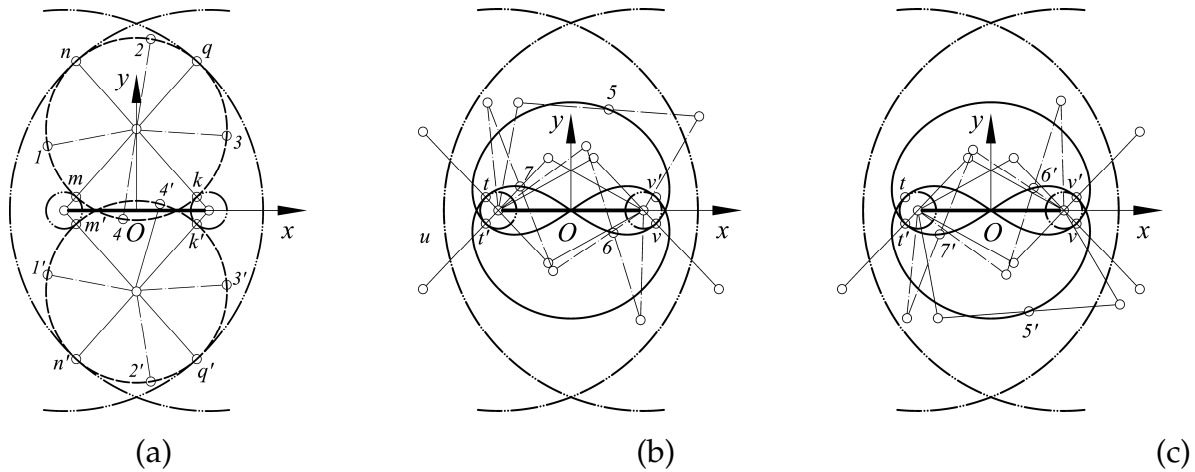


Fig. 13 The second kind of loci of a mechanism with different working modes

In this paper, we are just concerned about the mechanism with the working mode “+ -”. Fig. 14 shows the singular loci for all mechanisms with the working mode in the design space.

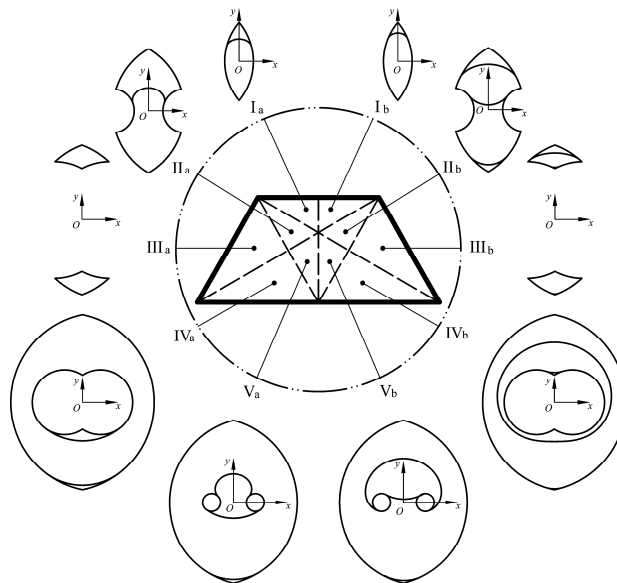


Fig. 14 Distribution of singular loci in the design space for the mechanism with the working mode “+ -”

4.4 Usable workspace

As we know, the practical workspace where a real mechanism works is different from the theoretical workspace. The region should contain no singular loci inside. From the distribution of theoretical workspace area and shape, one can see that the workspace area and shape of the mechanism with parameters $r_1 = 0.7$, $r_2 = 1.3$ and $r_3 = 1.0$ are identical to those of the mechanism with parameters $r_1 = 1.3$, $r_2 = 0.7$ and $r_3 = 1.0$. But from the analysis on singularity, the singularity loci for these two mechanisms are different. This will directly result in different usable workspaces. Therefore, based on Figs. 6 and 7, one cannot give any design result for a practical mechanism.

4.4.1 Definition

Usually, there exist singular loci inside the theoretical workspace (see Fig. 12). A mechanism wants to move from one point to another it maybe should pass a singular configuration. That means it should change from one working mode to another. In practice, changing working mode during the working process is definitely impossible. Therefore, we should find out a working space without singularity.

The *usable workspace* is defined as the maximum continuous workspace that contains no singular loci inside but bounded by singular loci outside. According to this definition, not every point within the usable workspace can be available for a practical mechanism. The mechanism will be out of control at the points on the boundaries and their neighborhoods. But within this region, the mechanism with a specified working mode can move freely.

The singular loci shown in Fig. 14 can be used to determine the usable workspace of a 5R parallel mechanisms with both the working mode “+ -” and the up-configuration. The workspace of a mechanism should be continuous. As shown in Fig. 14, the singular loci divide the theoretical workspace into several regions. The regions for the mechanisms in all sub-regions are separated. A practical mechanism cannot access the singular loci from one region to another. Even though, from Fig. 14, one can see that the two actuated links of the mechanism in sub-regions IVa, IVb, Va and Vb are both crank links. If one wants to find a mechanism that has two actuated crank links and has a surrounding workspace, he can select such a mechanism in these four sub-regions. However, in this paper we define the region above the x -axis as our usable workspace. For example, the usable workspace of the mechanism with $r_1 = 1.2$, $r_2 = 1.0$ and $r_3 = 0.8$ is shown as the hatched region in Fig. 15. Within this workspace, the mechanism has the configuration with both the inverse working mode “+ -” and the forward up-configuration. For the mechanism in one of the sub-regions Ia, Ib, IIa, IIb, IIIa and IIIb, the theoretical workspace above the x -axis is divided by the singular loci into several non-continuous regions, in which the region on the most top, where the mechanism is with the up-configuration, is considered as its usable workspace.

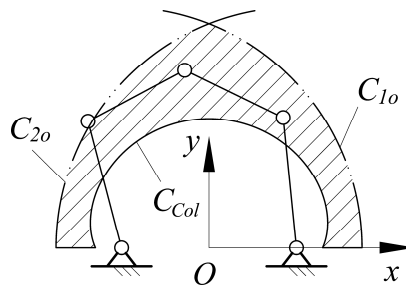


Fig. 15 The usable workspace of a mechanism

4.4.2 Distribution of the usable workspace shape in the design space

The usable workspace shape for the 5R parallel mechanism is classified in the design space as shown in Fig. 16. From the distribution one sees that

- In Fig. 16, each of the hatched regions is the usable workspace of the mechanism with the “+ -” working mode and the up-configuration, simultaneously.
- Each usable workspace is symmetric about the y -axis.
- The distribution in the design space is not symmetric about $r_1 = r_2$. The usable

workspace shape of a mechanism with $r_1 = a$, $r_2 = b$ ($a, b < 3$) and $r_3 = 3 - a - b$ is no longer the same as that of a mechanism with $r_1 = b$, $r_2 = a$ ($a, b < 3$) and $r_3 = 3 - a - b$.

- The usable workspace of a mechanism in sub-region IVa is half of its theoretical workspace.
- The flattest part in the workspace is always located at the region where $y = 0$.

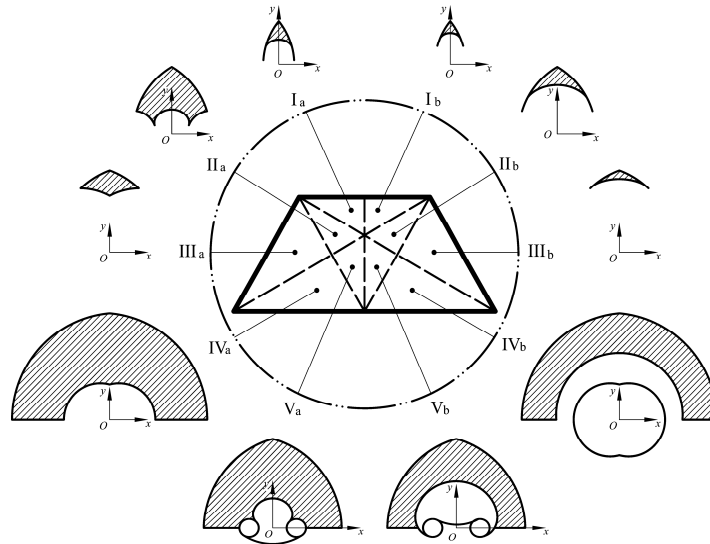


Fig. 16 The usable workspace shape in the design space

According to the definition, the usable workspace of a mechanism shown in Fig. 16 still cannot be used in practice since it is surrounded by singularities. At and near the boundary, the mechanism will be out of control. We should find a workspace in which every point or every pose is under control. Most importantly, we should find a solution to bound a workspace. In Refs. [9,16], a good-condition workspace or effective workspace was defined with respect to a specified minimum LCI. However, the minimum is still arbitrary or comparative since we cannot give it a definite value. Generally, it is not possible to define a mathematical distance to a singularity for a parallel mechanism [14]. Instead of LCI, here we will define an index by considering the force transmission, which is evaluated by the *transmission angle* in four-bar mechanisms.

5. Transmission Angle

5.1 Definition

The *transmission angle* is something we are very familiar with without realizing it. In everyday life, we frequently try to move an object that is somehow constrained, which cannot move freely but is attached to something: the handle of a crank, a curtain on a rail, a sliding door. In all of these cases, the object may not be able to move even when we exert pressure against it. Let's take the case of the handle of a crank as an example. As shown in Fig. 17, the crank is attached to the base with a constant counterclockwise moment M . To move it, we must apply a right-hand force F at the end of the crank. When the direction of the force is constant, depending on the position of the end point it will be more or less easy to start rotating. This is the reason why it sometimes feels comfortable and sometimes laborious when we ride a bicycle. This is actually a matter of the transmission angle. Since the direction of motion of a crank is always perpendicular to the crank, the smaller angle

between the force and crank is defined as the *transmission angle*, denoted as μ . When the force is normal to the crank, i.e. identical to the direction of motion, force transmission is most effective; when the force is perpendicular to the direction of motion, force transmission is very inefficient.

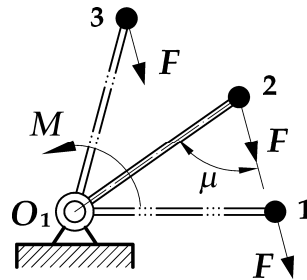


Fig. 17 The handle of a crank

For the planar four-bar mechanism shown in Fig. 18, if O_1A is the input link, the force applied to the output link BO_2 is transmitted through the coupler link AB . For sufficiently slow motions (negligible inertia forces), the force in the coupler link is pure tension or compression (negligible bending action) and is directed along AB . For a given force in the coupler link, the torque transmitted to the output bar (about point O_2) is at a maximum when the angle μ between the coupler bar AB and the output bar BO_2 is 90° . Therefore, angle ABO_2 is called the *transmission angle*. In [21], the transmission angle is defined as the smaller angle between the direction of the velocity difference vector of the driving link and the direction of the absolute velocity vector of the output link, both taken at the point of connection. Although there are other definitions (see [17,34], for instance), all these definitions are somehow related to a joint variable(s) of the mechanism.

When the *transmission angle* deviates significantly from 90° , the torque on the output bar decreases and may not be sufficient to overcome the friction in the system. For this reason, the deviation angle $\alpha = |90^\circ - \mu|$ should not be too great.

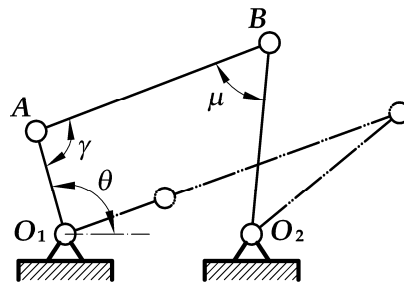


Fig. 18 Transmission angle

Meanwhile, at the moment that the angle γ between the input link O_1A and the coupler link AB is 0 or 180° , as shown in Fig. 18, the output point B will not move whatever the input is. Then, the motion of the input cannot be transmitted to the output effectively. This means the output point will lose a degree of freedom. Therefore, the deviation angle $\beta = |90^\circ - \gamma|$ should not be too great either. In this paper, the angle μ is defined as the *forward transmission angle*, and the angle γ is referred to as the *inverse transmission angle*. If BO_2 is an active link, the angle O_1AB is the *forward transmission angle* and angle ABO_2 the *inverse transmission angle*.

Take the slider-crank mechanism shown in Fig. 19 as an example, where angle $O'P_3B_3$

is the *forward transmission angle* and the angle between the coupler link and the normal to the straight-line path of the slider is the *inverse transmission angle* if the slider is actuated. For the 2-DOF 5R parallel mechanism shown in Fig. 1, the *forward transmission angle* is defined as the angle between the two couplers AP and PC [35]; and the *inverse transmission angle* is the angle between the input link and the coupler, as illustrated in Fig. 20. For the mechanism, there are two *inverse transmission angles*. By using the concept of *transmission angle*, as of 1961, the design of a 2-DOF five-bar mechanism has been investigated [36]. Recently, a synthesis method for the 5R variable topology mechanism has been proposed with transmission angle control [18].

5.2 Relationship between transmission angle and singularity

The *transmission angle* is an important index that can evaluate the quality of motion/force transmission. For this reason, the concept has been used in the design of almost all types of four-bar mechanisms, some other planar five-, six- and seven-bar mechanisms [37], the spatial four-link mechanisms [38] and even the 2-DOF spatial RSSRP mechanism [39].

Singularity is one of the most important problems in mechanisms, especially in parallel mechanisms. Since singularity leads to a loss of controllability and degradation of the natural stiffness, the analysis of parallel mechanisms has attracted considerable attention [4, 29, 40]. In a singularity, the condition number of the Jacobian matrix is normally null.

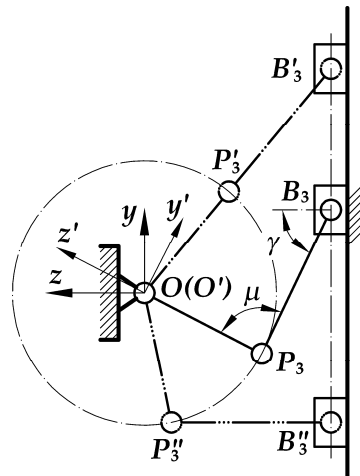


Fig. 19 Slider-crank mechanism

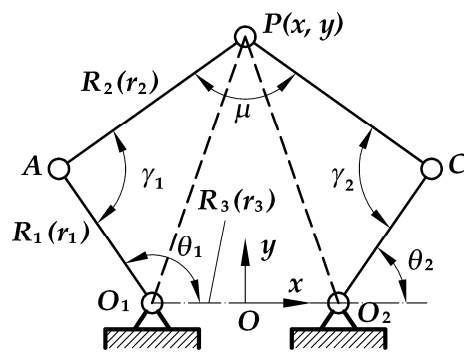


Fig. 20 The 5R parallel mechanism

There is a close relationship between the *transmission angle* and singularity. Taking the four-bar mechanism shown in Fig. 18 as an example, when $\mu = 0$ or 180° the

mechanism is in the “dead point” which is the second kind of singularity according to the classification in [4], while $\gamma=0$ or 180° corresponds to the first kind of singularity where the mechanism has the self-jamming characteristic. For the slider-crank mechanism shown in Fig. 19, the configuration $O'P'_3B'_3$ where $\mu=180^\circ$ is the second kind of singularity, whereas the configuration $O'P'_3B'_3$ where $\gamma=0$ is the first kind. The singularity of the 5R parallel mechanism shown in Fig. 20 has been listed systematically in section 4.3. One can see that $\gamma=0$ or 180° and $\mu=0$ or 180° represent the first and second kinds of singularities of the mechanism, respectively. Therefore, the *forward* and *inverse transmission angles*, μ and γ , are close relatives of the two kinds of singularities of the parallel mechanism. It is easy to conclude that if $\gamma=0$ or 180° and $\mu=0$ or 180° occur at the same time, the mechanism will be in the third kind of singularity. This case is not only architecture- but dimension-dependent as well.

In [41], the authors also investigated the relationship between pressure angle and singularity, and reached the conclusion that in the singularity the pressure is at 90° . However, according to their definition of pressure angles, their discussion was actually only about the second kind of singularity.

6. Definition of Some New Indices

6.1 Local Transmission Index (LTI)

The condition number of the Jacobian matrix is an index that has been used successfully in the design of serial robots. The condition number has the main advantage of describing the kinematic behavior of a robot by means of a number. The index has also been applied in the analysis and design of parallel mechanisms. It was used as an index to evaluate the accuracy/dexterity [10,11], to describe the closeness of a pose to a singularity of a parallel mechanism [42]. In an optimal design, the condition number (or its reciprocal) was used to define a useful, *good-condition* or *effective workspace* with a specified minimum [9,16]. However, the minimum is still arbitrary or comparative since we cannot give it a definite value. Generally, it is not possible to define a mathematical distance to a singularity for parallel mechanisms, whose DOF is a mix between translation and rotation [14].

Following the definition of transmission index proposed in [43], an index with respect to the *transmission angle* is defined as

$$\chi = \sin(TA) \quad (34)$$

where $TA = \mu$ or $TA = \gamma$. Then, there is

$$0 \leq \chi \leq 1 \quad (35)$$

A larger χ indicates better motion/force transmission. Since at a different pose the *transmission angles* will be different, the index χ is referred to as the *local transmission index* (LTI) in this paper. The angle is defined as the figure formed by two lines diverging from a common point, or as that formed by two planes diverging from a common line. Thus, the angle is usually measured by the ratio of two linear parameters. Therefore, the LCI is definitely independent of any coordinate frame. This is one of its advantages and is most important for the optimal design of mechanisms.

For the purpose of high speed and high quality of motion/force transmission, the most widely accepted ranges for the *transmission angle* are $(45^\circ, 135^\circ)$ [21] and $(40^\circ, 140^\circ)$ [17]. Therefore, the LTI limits will correspondingly be

$$\chi > \sin(\pi/4) \quad \text{and} \quad \chi > \sin(2\pi/9) \quad (36)$$

Then, unlike the LCI, the LTI has a significative limitation to its application.

6.2 Good-Transmission Workspace (GTW)

With the minimum of LTI, i.e. $\sin(\pi/4)$ or $\sin(2\pi/9)$, we can identify a workspace for any parallel mechanism. The corresponding workspace is referred to as a *good-transmission workspace* (GTW), which is defined as the set of pose where the transmission index for every *transmission angle* is greater than $\sin(\pi/4)$ or $\sin(2\pi/9)$. It is obvious that the minimum LTI, $\sin(2\pi/9)$, will lead to a larger GTW than $\sin(\pi/4)$.

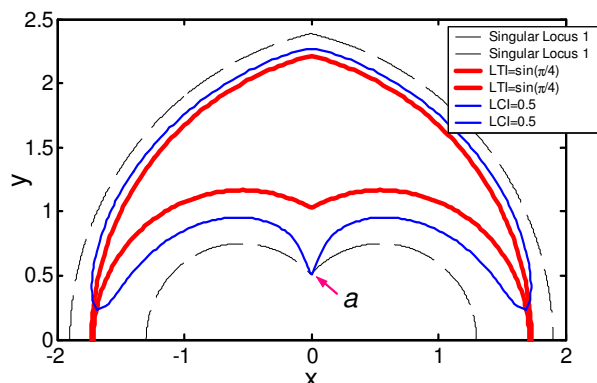
As an example, consider the planar 5R symmetrical parallel mechanism shown in Fig. 20. As analyzed in section 2, for a given position vector $\mathbf{p} = (x \ y)^T$ of the output point P , the position vectors $\mathbf{a}_{\mathfrak{R}}$, and $\mathbf{c}_{\mathfrak{R}}$, in the reference frame $\mathfrak{R}:O-xy$, of points A and C , respectively, can be obtained. Then, there are

$$\mu = \cos^{-1} \left(\frac{2r_2^2 - |\mathbf{a}_{\mathfrak{R}} \mathbf{c}_{\mathfrak{R}}|^2}{2r_2^2} \right) \quad (37)$$

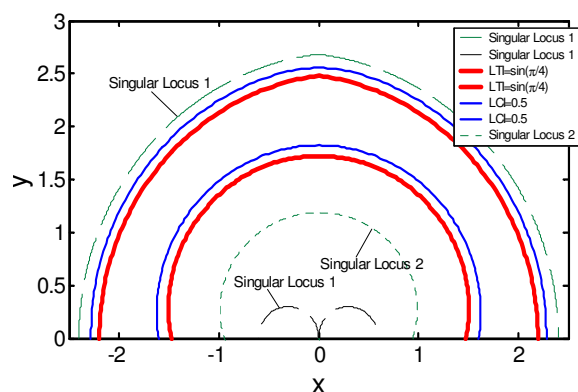
$$\gamma_i = \cos^{-1} \left(\frac{r_1^2 + r_2^2 - |\mathbf{o}_{i\mathfrak{R}} \mathbf{p}|^2}{2r_1 r_2} \right), \quad i=1,2 \quad (38)$$

where $\mathbf{o}_{i\mathfrak{R}}$ ($i=1,2$) are the position vectors of points O_i . By letting $\sin \mu > \sin(\pi/4)$ and $\sin \gamma_i > \sin(\pi/4)$, we can obtain the GTW of the mechanism numerically. This means, for a given position (x, y) of point P , to calculate the *forward* and *inverse transmission angles* μ and γ_i using Eqs. (37) and (38), if they all are subject to the LTI constraint given in Eq. (36), the point belongs to the GTW. For example, the GTW of the 5R parallel mechanism with parameters $r_1 = 0.85$, $r_2 = 1.6$ and $r_3 = 0.55$ is shown as the region bounded by the locus of $\text{LTI} = \sin(\pi/4)$ in Fig. 21(a). This normalized mechanism is an optimized solution when workspace, global conditioning index (GCI) and stiffness performances are the design indices [30]. According to the singular analysis result of the said paper, this mechanism does not have the second kind of singularity where points A , P and C are collinear. The region between the two loci of $\text{LTI} = \sin(\pi/4)$ in Fig. 21(b) is the GTW of the mechanism $r_1 = 1.5$, $r_2 = 1.2$ and $r_3 = 0.3$, which has the second kind of singularity. This non-dimensional mechanism is an optimum solution when workspace, GCI and velocity performances are all considered [30]. For comparison, in Fig. 21, the *good-condition workspace* specified by the loci of $\text{LCI} = 0.5$ (LCI is defined as the reciprocal of the condition number of the Jacobian matrix) is also illustrated. One may see that the two kinds of workspaces defined by LCI and LTI are different from others. There are two points we should notice. Firstly, from a given LCI we don't know how far the pose is from the singularity and we cannot even be sure whether the *good-condition workspace* (or the specified LCI value 0.5) is suitable or not. For example, as shown in Fig. 21(a), at and near the point a the LCI distribution is very dense. In this area, the points where $\text{LCI} = 0.5$ are very near to the singularity, while some other points with 0.5 are far from the singularity. However, the *transmission angle* has a definite physical significance. We can be sure that in the GTW defined by the LTI the motion/force transmission of the mechanism is effective. Secondly, for some points with a worse LCI value (for example less than 0.5 in the two examples), the mechanism is still effective in motion/force transmission. For example, Fig. 22 shows the configuration at the point $(1.7310, 0)$ of the mechanism with $r_1 = 0.85$,

$r_2 = 1.6$ and $r_3 = 0.55$, and all the *transmission angle* values. They all fall within the acceptable range ($45^\circ, 135^\circ$), but the LCI in this configuration is lower than 0.5 (see Fig. 21(a)). This means if we design a workspace, e.g. the *good-condition workspace*, with respect to the LCI, some points where the mechanism is good at motion/force transmission may be lost. Since the *transmission angle* has specific significance, we here prefer the design using the LTI.



(a)



(b)

Fig. 21 *Good-transmission workspace* of the 5R parallel mechanisms with the parameters (a) $r_1 = 0.85$, $r_2 = 1.6$ and $r_3 = 0.55$; (b) $r_1 = 1.5$, $r_2 = 1.2$ and $r_3 = 0.3$

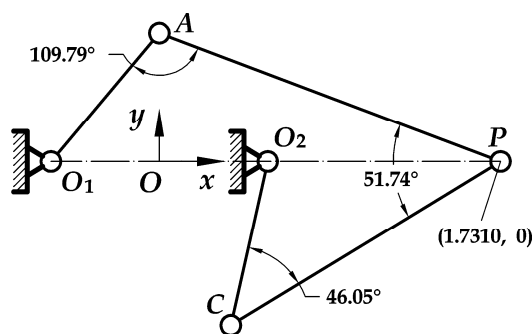


Fig. 22 One configuration of the 5R parallel mechanism

6.3 Global Transmission Index (GTI)

The LTI χ can only judge the effectiveness of motion/force transmission of a mechanism at a pose. In order to measure the global behavior of the motion/force transmission over the whole *good-transmission workspace* (GTW), a *global transmission index*

(GTI) is defined as

$$\Gamma = \frac{\int_W \sum_i^n \chi_i / n dW}{\int_W dW} \quad (39)$$

in which W denotes the GTW, n the number of transmission angles and $\Gamma_{\min} < \Gamma < 1$ (Γ_{\min} equals $\sin(\pi/4)$ or $\sin(2\pi/9)$). It is obvious that the GTI is also independent of any coordinate frame.

7. Performance chart of the 2-DOF 5R parallel mechanism

As is well known, a performance chart (atlas) can show the relationship between a performance index and associated design parameters in a limited space, globally and visually. The design method by using the performance chart (atlas) has been widely used in the classical mechanical design and most design manuals. Here, performance charts of the indices for the 2-DOF 5R parallel mechanism will be presented in this section. Some of them will be used in the optimization of the mechanism.

7.1 Distribution of the GTW shape in the design space

Letting $\sin \mu > \sin(\pi/4)$ and $\sin \gamma_i > \sin(\pi/4)$, one can numerically obtain the good-transmission workspace (GTW) of a 2-DOF 5R parallel mechanism. The GTW for the 5R parallel mechanisms is classified in the design space as shown in Fig. 23. From the distribution one sees that

- In Fig. 23, each of the hatched regions is the GTW of the mechanism with the “+ –” working mode and the up-configuration, simultaneously.
- For some mechanisms, especially those in the sub-regions Ia, Ib, IIb and IIIb, their GTWs are zero.
- Each GTW is symmetric about the y -axis.
- The distribution in the design space is not symmetric about $r_1 = r_2$.
- The fattest part in the workspace is always located at the y -axis.

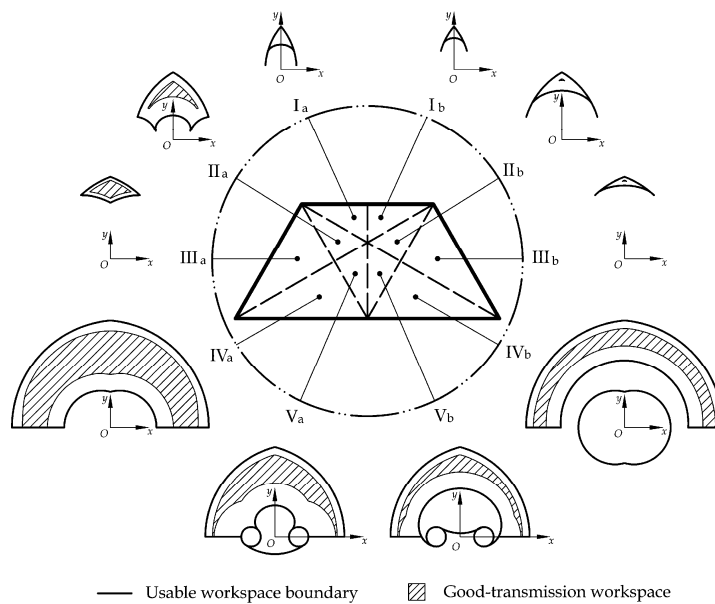


Fig. 23 The GTW shape in the design space

7.2 Performance chart of the GTW

According to the definition of GTW in Sec. 6.2, it is possible to calculate the GTW of any one non-dimensional mechanism in the parameter design space shown in Fig. 4(b). The performance chart illustrating the relationship between the normalized parameters r_i ($i=1, 2, 3$) and the GTW, letting $\sin \mu > \sin(\pi/4)$ and $\sin \gamma_i > \sin(\pi/4)$, is illustrated in Fig. 24, from which we may see that (a) the index is inversely proportional to the parameter r_3 when r_2 is specified, and (b) the GTW of some mechanisms in the design space is zero.

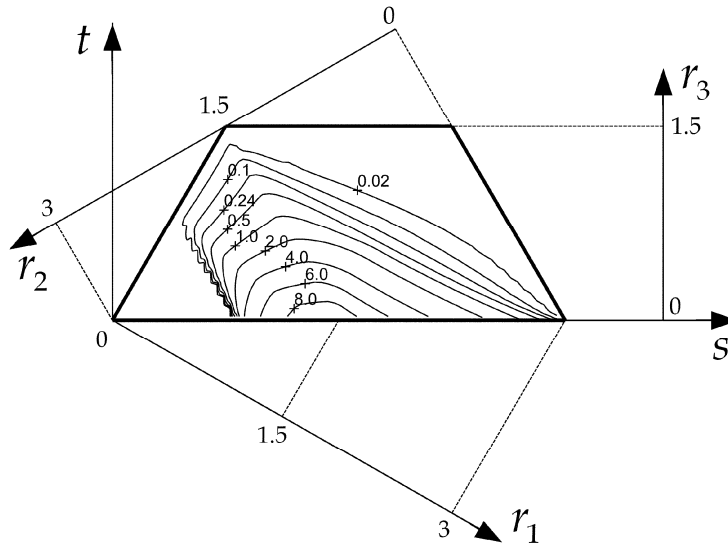


Fig. 24 Performance chart of the *good-transmission workspace* (GTW)

7.3 Performance chart of the GTI

By using the Eq. (39) and the GTW result, we can also represent the relationship between the GTI and the non-dimensional mechanisms in the parameter design space shown in Fig. 4(b). The corresponding performance chart is illustrated in Fig. 25, which shows that, in the design space, the mechanisms near the area $r_2 = 1.69$ usually have better GTI performance.

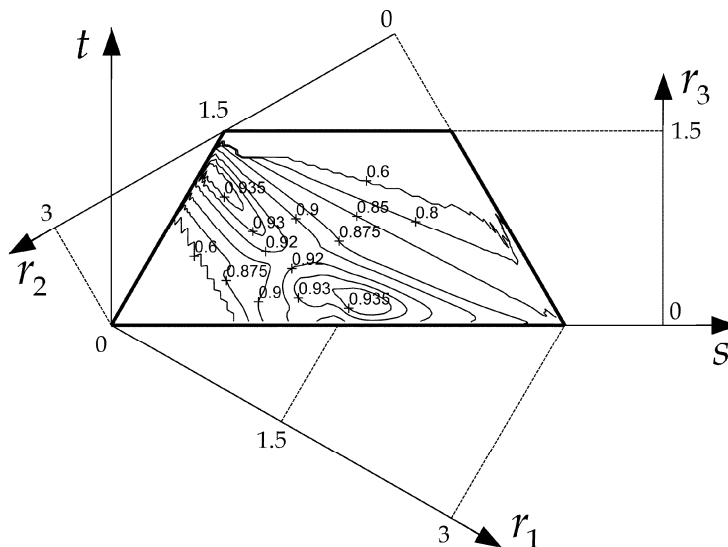


Fig. 25 Performance chart of the *global transmission index* (GTI)

7.4 Performance chart of the fatness index (FI) of the GTW

7.3.1 Definition of the fatness index (FI)

From Fig. 23, one may see that with different link lengths the GTW shape may be different. The GTW of some mechanisms is in a narrow shape, while for some mechanisms it is broad. Comparing Figs. 23 and 24, we may observe that a GTW with larger volume does not mean broad, whereas a GTW with smaller volume may be in a broad shape.

Undoubtedly, in some applications a narrow or circular workspace will be required. However, in some industrial applications, a regular workspace such as a rectangular or foursquare workspace is needed. For this case, a broader workspace is welcome. For this purpose, we here should introduce an index to evaluate the fatness of the GTW. From Fig. 23, one may see that the fattest part in the GTW is always located at the y -axis. In this paper, the GTW length along the y -axis, denoted as d_y , is defined as the *fatness index* (FI) of the GTW. The larger the FI value, the broader the GTW.

It is undoubted that two mechanisms with same GTW volumes may have different FIs. For example, Fig. 26 (a) and (b) show the GTW of a mechanism with $r_1 = 1.57$, $r_2 = 1.161$ and $r_3 = 0.269$, and that of a mechanism with $r_1 = 0.795$, $r_2 = 1.93$ and $r_3 = 0.275$, respectively. The volume of both of them is 4.0, however, their FIs are different, $d_{y1} = 0.7$ and $d_{y2} = 0.95$.

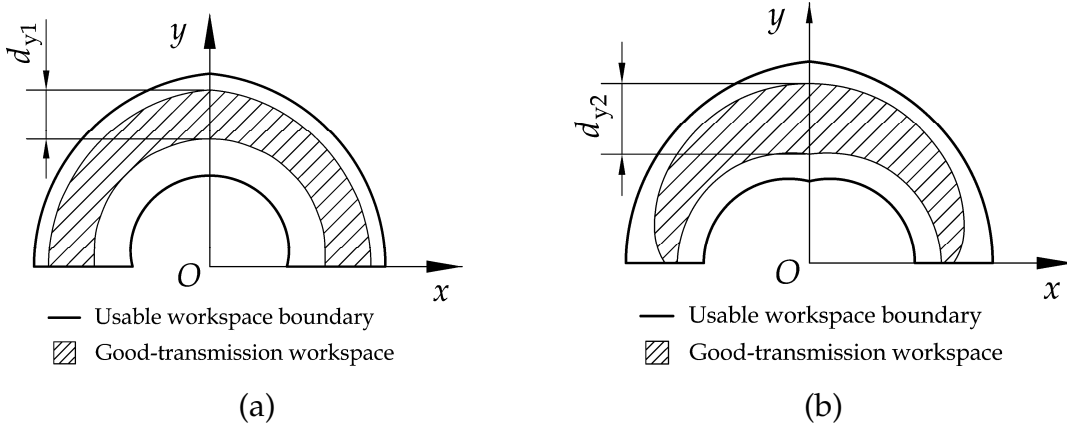


Fig. 26 GTW and fatness index of two mechanisms with: (a) $r_1 = 1.57$, $r_2 = 1.161$ and $r_3 = 0.269$; and (b) $r_1 = 0.795$, $r_2 = 1.93$ and $r_3 = 0.275$

7.3.2 Performance chart of the fatness index

Figure 27 illustrates the FI performance chart of the 2-DOF 5R parallel mechanisms. It shows that the index is inversely proportional to the parameter r_3 when r_2 is specified. The performance chart can be used in the optimization of the mechanism if a regular workspace is required in a practical design.

8. Optimization process

8.1 Relationship between a non-dimensional mechanism and its corresponding dimensional mechanism

In the design space, the parameters r_1 , r_2 and r_3 have no dimension. They are the ratios of the dimensional parameters R_i to a dimensional scale D , which is the average of R_1 , R_2 and R_3 as shown in Eq. (13). As given in Eq. (16), the parameters r_1 , r_2 and

r_3 are limited. But each of the parameters R_1 , R_2 and R_3 can be infinite. Practically, we are concerned with the dimensional mechanism but not the non-dimensional one. But it is not difficult to find that the ratio $R_1 : R_2 : R_3$ is always equal to $r_1 : r_2 : r_3$. For any possible dimension combination of R_1 , R_2 and R_3 , one can always find its corresponding group of r_1 , r_2 and r_3 in the design space. The design space defined by r_1 , r_2 and r_3 makes it possible for us to investigate the performance of all possible 5R parallel mechanisms. For example, the performance chart of Fig. 27 shows the global result about the fatness of GTW, which can characterize the GTW with the help of Figs. 23 and 24. From Figs. 23, 24 and 27, we can know the GTW result of a non-dimensional 5R parallel mechanism. Then, how about the dimensional mechanisms? We know that the key coefficient between R_i and r_i is the dimensional scale D . Once we select a suitable group of r_1 , r_2 and r_3 , the parameter D will lead it to a dimensional mechanism by Eq. (14). The problem is how the GTW of the dimension mechanism will be if one knows that of a non-dimensional mechanism from Figs. 23, 24 and 27.

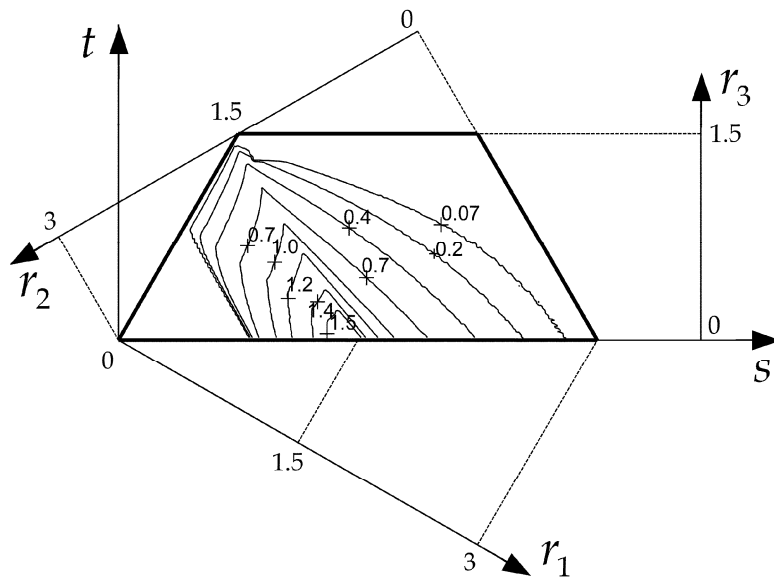


Fig. 27 Performance chart of the *fatness index* (FI) for GTW

Angle is defined as the figure formed by two lines diverging from a common point, or as that formed by two planes diverging from a common line. Thus, the angle is usually measured by the ratio of two linear parameters. In this paper, the transmission angle is used to define the index LTI. And we use the LTI limit, i.e. $\sin(\pi/4)$, to identify the GTW. Therefore, the GTW shape of a mechanism with R_i will be similar to that of its corresponding non-dimensional mechanism with r_i , and their GTW volumes will have the relationship as following

$$GTW_D = D^2 GTW_{\text{non-D}} \quad (40)$$

in which GTW_D and $GTW_{\text{non-D}}$ denote the GTW volumes of the dimensional mechanism with parameters R_i and its corresponding non-dimensional mechanism with parameters r_i , respectively. However, from Eq. (39), we may see that their GTI values will be the same.

Therefore, all mechanisms with parameters $R_i = Dr_i$ have similar performances to that with the non-dimensional parameters r_i . For example, the GTW of the mechanism

with R_i is D^2 -time that of the mechanism with r_i . Within the similar workspaces, the GTI values are the same as that of the other. The mechanisms, which have such a performance similarity, are referred to as the *similarity mechanisms* (SMs). Then, the ratios of geometric parameters R_i of all SMs are constant. Any one of the non-dimensional mechanisms in the parameter design space stands for all of its possible SMs. Therefore, the mechanisms with parameters r_i are defined as *basic similarity mechanisms* (BSMs). After normalization, a mechanism with any kind of link lengths can find its position or its BSM in the design space. For such a reason, the design space is a useful tool to present a global comparative result in terms of performances for all mechanisms. This also guarantees a global optimum result in the design issue, and the performance charts can be used in the optimization. Since the BSMs are in a limited space, i.e. the parameter design space, in the design process we should first be concerned about the BSMs.

8.2 Optimization by using the performance charts

The objective of optimization is to determine the geometrical parameters of a mechanism for a desired workspace. In this process, such other performances may be considered. For the parallel mechanism studied here, the optimization taking into account the desired workspace and force transmissibility based on the performance charts in Sec. 7 can be summarized as follows:

Step 1: Identify an optimum region in the *parameter design space*. The identification of optimum region is depended on the design requirement. For different practical design, the optimum region may be different. Anyway, we usually would like the mechanism candidate to have a workspace as large as possible. For this case, we can identify an optimum region with large GTW and better GTI. For example, letting $GTW \geq 5.0$ and $GTI \geq 0.925$, an optimum region denoted as $\Omega_{GTW-GTI}$ can be identified (shown as the hatched region in Fig. 28(a)) by using the performance charts of Figs. 24 and 25. The optimum region $\Omega_{GTW-GTI}$ contains all possible optimum solutions with the non-dimensional parameters r_i ($i=1, 2, 3$). However, the optimum region is not unique. It can be changed when the constraints are different. For example, if we would like to reduce the optimum region, we can use stricter constraints, such as $GTW \geq 6.0$ and $GTI \geq 0.93$. The optimum region denoted as $\Omega'_{GTW-GTI}$ is shown in Fig. 28(b).

For a practical design that a regular workspace is required, the fatness of GTW should be considered. The corresponding optimum region can be identified by using the performance charts shown in Figs. (24), (25) and (27). For example, letting $GTW \geq 6.0$, $GTI \geq 0.93$ and $FI \geq 1.2$, an optimum region denoted as $\Omega_{GTW-GTI-FI}$ can be obtained as shown in Fig. 29.

Step 2: Select a solution candidate, i.e. BSM, from the optimum region. The optimum region obtained contains all possible solutions with better performances. Since there is no best but only a comparatively better solution for a design problem, we can pick any non-dimensional mechanism from the region. For example, the BSM with parameters $r_1 = 1.25$, $r_2 = 1.49$ and $r_3 = 0.26$ is selected here from the optimum region $\Omega_{GTW-GTI-FI}$. The GTW, GTI and FI of the mechanism are 6.4125, 0.9337 and 1.3911, respectively. Fig. 30 shows the mechanism, its GTW and the distribution of LTI within the GTW.

Step 3: Determine the dimensional parameters R_i . According to Eq. (14), we first need to determine the normalization factor D . As described in [25], this factor can be

obtained by comparing the desired workspace of a design problem to the workspace of the non-dimensional mechanism selected from the optimum region. Therefore, how much the normalization factor D will be depends on the desired workspace. Once the desired workspace is given, the factor can be calculated by using Eq. (40). For example, if the desired workspace is similar to the GTW shown in Fig. 30 and its volume $GTW_D=200\text{mm}^2$, since $GTW_{\text{non-D}}=6.4125$, then $D=\sqrt{GTW_D/GTW_{\text{non-D}}}\approx 5.5847\text{mm}$. Rewriting Eq. (14) as $R_i = Dr_i$, then $R_1=5.5847\text{mm} \times 1.25\approx 6.98\text{mm}$, $R_2=5.5847\text{mm} \times 1.49\approx 8.32\text{mm}$, and $R_3=5.5847\text{mm}\times 0.26\approx 1.45\text{mm}$.

For the above example, as shown in Fig. 30, an included rectangular workspace with the volume $2.2072(\text{length})\times 0.9815(\text{width})\approx 2.16$ can be identified in the GTW. Then, there must exist a similar workspace in the whole GTW of the dimensional mechanism with $R_1=6.98\text{mm}$, $R_2=8.32\text{mm}$, and $R_3=1.45\text{mm}$. Its volume should be $D^2\times 2.17=(D\times 2.2072)\times (D\times 0.9815)\approx 67.56\text{mm}^2$. This means that, if a rectangular workspace is desired in a practical design, one should first find an included rectangle in the GTW of the selected BSM by taking into account the desired workspace.

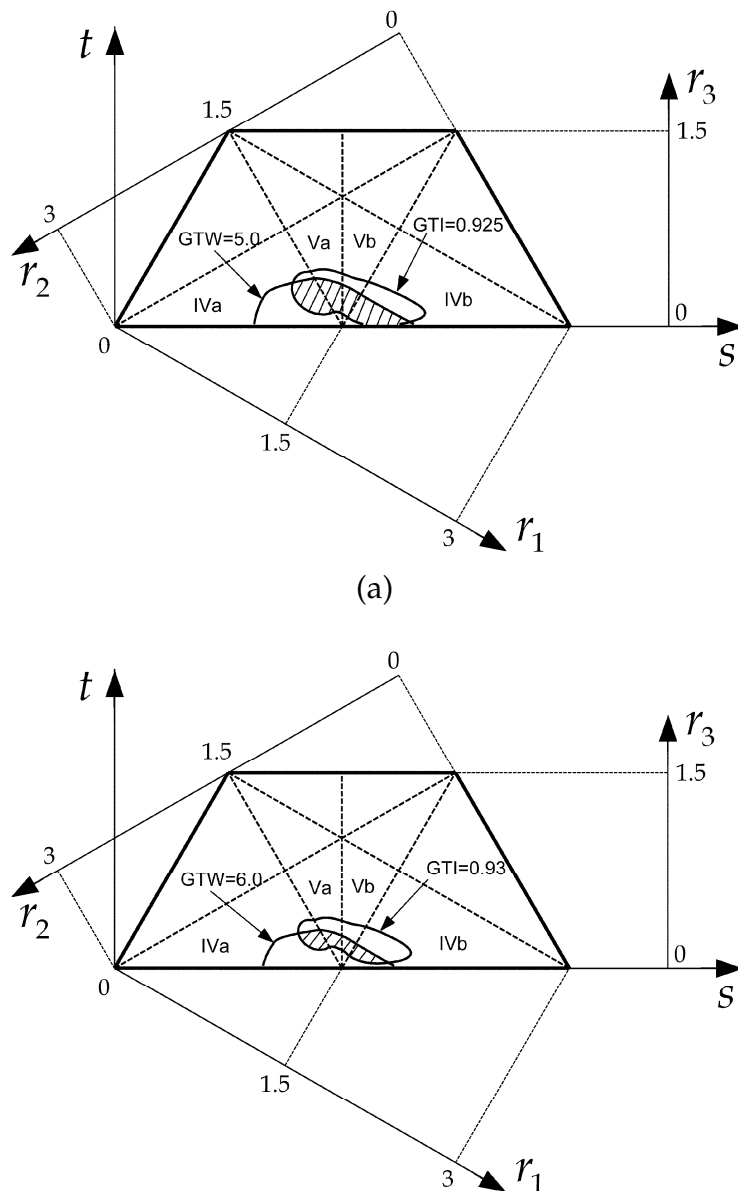


Fig. 28 Optimum regions for the 2-DOF 5R parallel mechanism when (a) $GTW\geq 5.0$ and

GTI \geq 0.925, and (b) GTW \geq 6.0 and GTI \geq 0.93

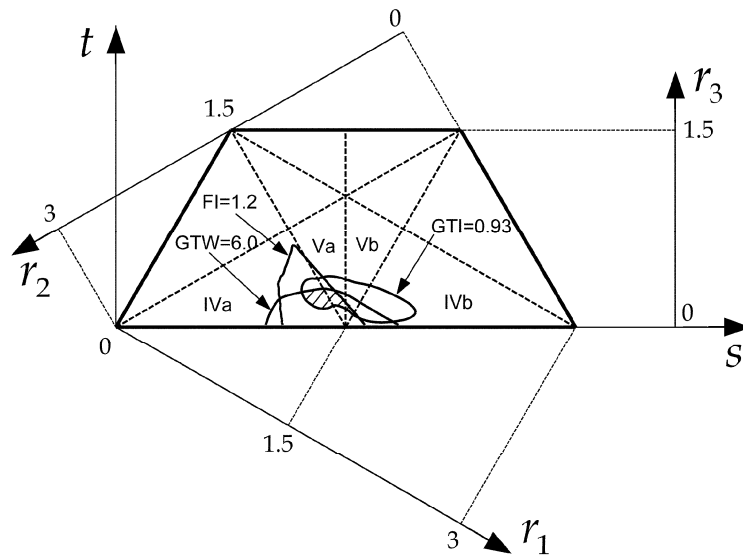


Fig. 29 An optimum region for the 2-DOF 5R parallel mechanism when GTW \geq 6.0, GTI \geq 0.93 and FI \geq 1.2

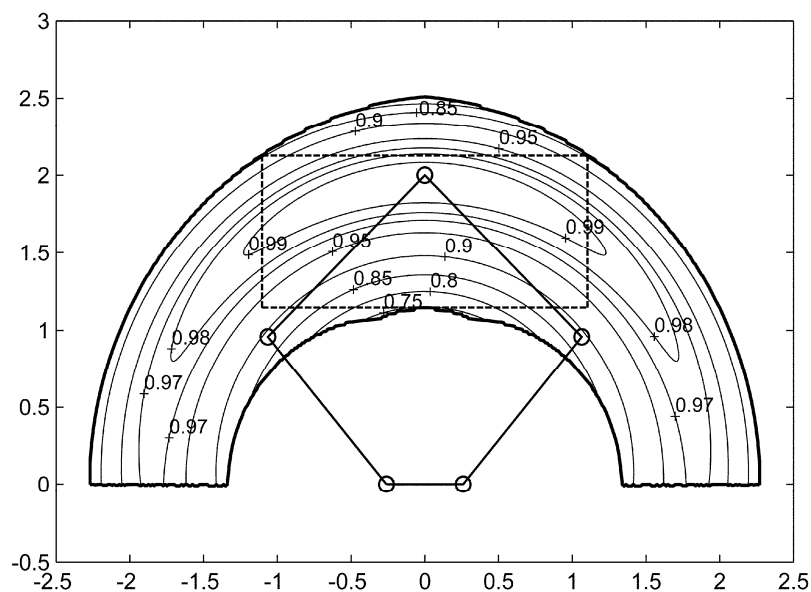


Fig. 30 Mechanism, GTW, LTI distribution, and included rectangular workspace of one optimum BSM

Step 4: Check whether the dimensions obtained in Step 3 is enough or not for a practical design, and, if necessary, revise the design solution. In the previous step, we determined the dimensional parameters, which are $R_1=6.98\text{mm}$, $R_2=8.32\text{mm}$, and $R_3=1.45\text{mm}$. In this step, one must check the dimensions to make it sure that all components can be placed well and any other item needed in the practical design problem is feasible. If it is okay, proceed to Step 5; otherwise, return to Step 2 and pick up another group of non-dimensional parameters from the optimum region, and repeat Steps 3 and 4.

Step 5: Calculation of the input range. The input range required to reach the desired workspace of the optimized mechanism can be calculated by means of the inverse

kinematics of Eq. (6). For example, for the solution obtained in Step 3, the input ranges are $\theta_1 \in [-13.68^\circ, 97.64^\circ]$ and $\theta_2 \in [82.36^\circ, 193.68^\circ]$ for the desired workspace of $12.3265(\text{length}) \times 5.4813(\text{width}) \approx 67.56 \text{mm}^2$.

Step 5: Finish the optimization problem.

From the above process, one may see that the design method may provide all possible solutions since it gives an optimum region not just one solution, and allows the designer to adjust his design solution. They are actually the advantages of this approach.

9. Conclusions

In this paper, the kinematic analysis and optimization problems for the 2-DOF 5R symmetrical parallel mechanisms are addressed again by taking into account the concept of force transmissibility. Firstly, it shows that the theoretical workspace cannot be used practically due to the inside singularity. The usable workspace without singularity inside cannot be useful in an optimization problem either since a mechanism at and near the boundary of the workspace will be out of control. Additionally, the local conditioning index (LCI), which is widely used in the field of serial robots and has been applied in many optimizations, has the problem of physical significance and difficulty of measuring the distance to a singularity of a parallel mechanism. The usable workspace limited by a specified LCI is then doubtful.

Since the transmission angle that can evaluate the force transmissibility of planar four-bar mechanisms, the concept is applied into the analysis of the 5R parallel mechanisms in this paper. Three new indices, i.e. the local transmission index (LTI), good-transmission workspace (GTW) and global transmission index (GTI), are introduced accordingly. It shows that the LTI, unlike the LCI, has a valuable significance to its application. That is, it can evaluate the force transmissibility of a mechanism. In addition, the fatness index (FI) that is used to measure the fatness of a GTW is also proposed here.

Finally, based on the performance charts of GTW, GTI and FI, the optimization process of determining the link lengths of the 5R parallel mechanism is presented accordingly. The method may not only provide all possible optimum solutions but allow the designer to adjust his solution.

The application of three new indices, i.e. LTI, GTW and GTI, shall be said to be extended to other parallel mechanisms.

Acknowledgement

This work was supported by the National Natural Science Foundation of China under Grant 50505023, by the High Technology Research and Development Program (863 Program) of China (No. 2006AA04Z227), and partly by the National Basic Research Program (973 Program) of China (No. 2006CB705400), and was partly carried out during a one-month visit by the first author to the Fraunhofer Institute for Machine Tools and Forming Technology IWU, Chemnitz, Germany, in the summer of 2007 supported by the Ministry of Education of China and the Deutsche Forschungsgemeinschaft.

References

1. K.M. Lee and D.K. Shah, Part 1: Kinematic analysis of a 3-DOF in-parallel actuated manipulator, *IEEE Journal of Robotics and Automation* 4 (1988) 354-360.
2. J.-P. Merlet, Direct kinematic and assembly motion parallel manipulators, *Int. J. Robotics Research* 11 (2) (1992) 150-162.
3. J.P. Merlet, C.M. Gosselin and N. Mouly, Workspace of planar parallel manipulators,

- Mech. Mach. Theory 33 (1/2) (1998) 7-20.
4. C.M. Gosselin and J. Angeles, Singularity analysis of closed loop kinematic chains, *IEEE Trans. on Robotics and Automation* 6 (3) (1990) 281-290.
 5. X.-J. Liu, J. Wang, F. Gao and L.-P. Wang, On the analysis of a new spatial three degrees of freedom parallel manipulator, *IEEE Transactions on Robotics and Automation* 17 (6) (2001) 959-968.
 6. I.A. Bonev, D. Zlatanov, C. M. Gosselin, Singularity analysis of 3-DOF planar parallel mechanisms via screw theory, *ASME Journal of Mechanical Design* 125 (2003) 573-581.
 7. C.M. Gosselin and J. Angeles, The optimum kinematic design of a spherical three degree-of-freedom parallel manipulator, *J. Mech. Transm. Autom. Des.* 111 (1989) 202-207.
 8. E. Ottaviano and M. Ceccarelli, Optimal design of CaPaMan (Cassino Parallel Manipulator) with a specified orientation workspace, *Robotica* 20 (2002) 159–166.
 9. X.-J. Liu, Optimal kinematic design of a three translational DOFs parallel manipulator, *Robotica* 24 (2) (2006) 239-250.
 10. C. M. Gosselin, The optimum design of robotic manipulators using dexterity indices, *Robotics and Autonomous Systems* 9 (1992) 213-226.
 11. R.S. Stoughton and T. Arai, A modified Stewart platform manipulator with improved dexterity, *IEEE Transactions on Robotics and Automation* 9 (2) (1993) 166-173.
 12. J. Ryu and J. Cha, Optimal architecture design of parallel manipulators for best accuracy, in: *Proceedings of the 2001 IEEE/RSJ International Conference on Intelligent Robots and Systems*, Maui, Hawaii, USA, 2001, pp. 1281-1286.
 13. H. S. Kim, and L.-W. Tsai, Design optimization of a Cartesian parallel manipulator, *Journal of Mechanical Design* 125 (1) (2003) 43-51.
 14. J. P. Merlet, Jacobian, manipulability, condition number, and accuracy of parallel robots, *Journal of Mechanical Design* 128 (2006) 199-206.
 15. C. Gosselin, J. Angeles, A global performance index for the kinematic optimization of robotic manipulators, *Journal of Mechanical Design* 113 (1991) 220-226.
 16. Y.J. Lou, G.F. Liu, N. Chen, and Z.X. Li., Optimal design of parallel manipulators for maximum effective regular workspace, in: *Proc. of IEEE/RSJ International Conference on Intelligent Robots and Systems*, Edmonton, Canada, 2005, pp.1208-1213.
 17. H. Alt, Der Übertragungswinkel und seine Bedeutung für das Konstruieren periodischer Getriebe, *Werkstatttechnik* 26 (Heft 4) (1932) 61-65.
 18. S. S. Balli and S. Chand, Transmission angle in mechanisms, *Mechanism and Machine Theory* 37(2002) 175-195.
 19. P.W. Eschenbach and D. Tesar, Link length bounds on the four bar chain, *J. Eng. Ind. Trans. ASME Ser. B* 93(1971) 287-293.
 20. A.S. Hall, *Kinematics and linkage design*, Prentice-Hall, Englewood Cliffs, NJ, 1961, pp.41.
 21. R.S. Hartenberg, J. Denavit, *Kinematic synthesis of linkages*, McGraw-Hill, New York, 1964, pp. 46-47.
 22. D.C. Tao, *Applied linkage synthesis*, Addison-Wesley, Reading, MA, 1964, pp.7-12.
 23. J.T. Kimbrell, *Kinematics analysis and synthesis*, McGraw-Hill, NY, 1991, pp.14-15.
 24. G. H. Sutherland and J. N. Siddall, Dimensional synthesis of linkage by multifactor optimization, *Mechanism and Machine Theory* 9 (1974) 81-95.
 25. X.-J. Liu and J. Wang, A new methodology for optimal kinematic design of parallel mechanisms, *Mechanism and Machine Theory*, Vol.42, No.9, pp.1210-1224, 2007.
 26. G. Alici, An inverse position analysis of five-bar planar parallel manipulators,

- Robotica 20 (2002) 195-201.
27. X.-J. Liu, J. Wang and G. Pritschow, Kinematics, singularity and workspace of planar 5R symmetrical parallel mechanisms, *Mechanism and Machine Theory*, Vol.41, No.2, pp.145-169, 2006.
 28. J. J. Cervantes-Sánchez, J. C. Hernández-Rodríguez and J. G. Rendón-Sánchez, On the workspace, assembly configurations and singularity curves of the RRRRR-type planar manipulator, *Mechanism and Machine Theory* 35 (2000) 1117-1139.
 29. F.C. Park and J.W. Kim, Singularity analysis of closed kinematic chains, *Journal of Mechanical Design* 121 (1999) 32-38.
 30. X.-J. Liu, J. Wang and G. Pritschow, Performance atlases and optimum design of planar 5R symmetrical parallel mechanisms, *Mechanism and Machine Theory*, Vol.41, No.2, pp.119-144, 2006.
 31. J. J. Cervantes-Sánchez, J. C. Hernández-Rodríguez and J. Angeles, On the kinematic design of the 5R planar, symmetric manipulator, *Mechanism and Machine Theory* 36 (2001) 1301-1313.
 32. G. Alici and B. Shirinzadeh, Optimum synthesis of planar parallel manipulators based on kinematic isotropy and force balancing, *Robotica* 22 (2004) 97-108.
 33. I.A. Bonev and C.M. Gosselin, Singularity loci of planar parallel manipulators with revolute joints, 2nd Workshop on Computational Kinematics, Seoul, South Korea, May 20-22, 2001.
 34. K. Hain, *Applied kinematics*, McGraw-Hill, NY, 1967.
 35. K.L. Ting and G.H. Tsai, "Mobility and synthesis of five-bar programmable linkages," in *Proceedings of 9th OSU Applied Mechanisms Conference*, Kanas City, MD, 1985, pp.III-1-III-8.
 36. R. Stanley, "Five-bar loop synthesis," *Mach. Design*, pp.189-195, 1961.
 37. M.R.E. Philipp and F. Freudenstein, "Synthesis of two-degree-of-freedom linkages—a feasibility study of numerical methods of synthesis of bivariate function generators," *Journal of Mechanisms*, vol. 1, pp.9-21, 1965.
 38. E. Söylemez and F. Freudenstein, "Transmission optimization of spatial 4-link mechanisms," *Mechanism and Machine Theory*, vol. 17, pp.263-283, 1982.
 39. R.I. Alizade, A.V. Mohan Rao, G.N. Sandor, "Optimum synthesis of two degree of freedom planar and spatial function generating mechanism using the penalty function approach," *J. Eng. Ind. Trans. ASME*, pp.629-634, 1975.
 40. G. Liu, Y. Lou, and Z. Li, "Singularities of parallel manipulators: a geometric treatment," *IEEE Transactions on Robotics and Automation*, vol. 19, pp. 579-594, 2003.
 41. H. Funabashi and Y. Takeda, "Determination of singular points and their vicinity in parallel manipulators based on the transmission index," in *Proc. 9th World Congress on the Theory of Machines and Mechanisms*, Milan, Italy, 1995, pp. 1977-1981.
 42. P. A. Voglewede and I. Ebert-Uphoff, "Measuring 'closeness' to singularities for parallel manipulators," in *Proc. IEEE Int. Conf. on Robotics and Automation*, New Orleans, 2004, pp. 4539-4544.
 43. G. Sutherland and B. Roth, "A transmission index for spatial mechanism," *J. Eng. Ind. Trans. ASME*, pp.589-597, 1973.